Int. J. Electrochem. Sci., 16 **(2021)** Article Number: 211146, doi: 10.20964/2021.11.22

International Journal of
ELECTROCHEMICAL
SCIENCE
www.electrochemsci.org

Machine Learning Aided Discovery of the Layered Double Hydroxides with the Largest Basal Spacing for Super-Capacitors

Kailiang Lu[1], *Dongping Chang*[1], *Xiaobo Ji*[2], *Minjie Li*[2,*], *Wencong Lu*[1,2,*]

[1] Materials Genome Institute, Shanghai University, Shanghai 200444, China
[2] Department of Chemistry, College of Sciences, Shanghai University, Shanghai 200444, China
[*]E-mail: wclu@shu.edu.cn

Received: 29 July 2021 / *Accepted:* 12 September 2021 / *Published:* 10 October 2021

Super capacitors with layered double hydroxides (LDHs) have excellent specific capacitance and cycling performance due to their unique layered structures and rich REDOX sites. The basal spacing ($d_{spacing}$) of LDHs can be controlled by selecting optimal metal cations and interlayer anions. In general, the greater the $d_{spacing}$ of LDHs electrode materials, the greater the specific capacitance of the super-capacitors. In this work, the machine learning model was utilized to seek for novel LDHs materials with the larger $d_{spacing}$. The genetic algorithm combined machine learning approaches were utilized to select the appropriate feature subset including atomic parameters and chemical compositions of LDHs. The Extreme Gradient Boosting model was established to predict the $d_{spacing}$ of LDHs. The correlation coefficient between predicted $d_{spacing}$ and experimental $d_{spacing}$ reached as high as 0.94 for the training set in leave-one-out cross-validation (LOOCV) and 0.89 for the independent testing set, respectively. The high-throughput screening of new LDHs with larger $d_{spacing}$ was carried out by using our online computation platform for materials data mining (OCPMDM). The $d_{spacing}$ of designed LDHs ($Co_{0.67}Fe_{0.33}[Fe(CN)_6]_{0.11}\bullet(OH)_2$) was predicted to be 12.40*Å*, increasing by 10.91% compared to the maximum $d_{spacing}$ (11.18*Å*) of $Mg_{0.67}Al_{0.33}$ $[Fe(CN)_6]_{0.08}\bullet(OH)_2$ reported. The online platform for predicting $d_{spacing}$ of unknown LDHs can be accessible for the public on the web server: http://materials-data-mining.com/online_model/LDHs_basal_spacing_model.

Keywords: Layered double hydroxides; Basal spacing; Machine learning; High-throughput screening; Material design

1. INTRODUCTION

Considering the current environmental protection problem and shortage of energy, the energy storage field was widely concerned owe to the probability of clean energy power generation. [1-5] Energy storage devices include conventional capacitors, fuel cells, rechargeable batteries, and super-

capacitors. Super-capacitors are new components that store energy through a two-layer interface between an electrode and an electrolyte. Super-capacitor has drawn great concern in recent years owe to long cycle life, high specific capacitance, excellent reliability, and wide operating temperature. [6-10] In view of different storage energy mechanisms, super-capacitors can be divided into two categories: electrochemical double-layer capacitors (EDLCs) based on carbon and pseudo-capacitors based on metal oxides/hydroxides or electronically conducting polymers. [11] Pseudo-capacitors mainly generate pseudo-capacitance through the reversible REDOX reaction on the surface of the active electrode material to realize the storage and conversion of energy. The specific capacitance of the pseudo-capacitors is tens of times larger than that of EDLCs by using interfacial reversible faradaic reactions. Traditional pseudo-capacitor materials mainly include typical transitional metal oxides/hydroxides, such as RuO_2, MnO_2, Co_3O_4, NiO, Fe_3O_4, $Ni(OH)_2$, $Co(OH)_2$, and their binary systems. [6] Recently, layered double hydroxides (LDHs) were regarded as the electrode material for super-capacitors due to their layered structures.

LDHs are the type of two-dimensional nanostructured anionic clays with commutable anions in the interlayer space composed of two kinds of metallic cations. [12] LDHs may be represented by the general formula$[M_{1-x}^{2+}M_x^{3+}(OH)_2]^{x+}(A^{n-})_{x/n}$, where M^{2+}(M = e.g. Mg, Cu, Ni, Co, Cd, or Zn) and M^{3+}(M = e.g. Al, Ga, Cr, Fe or In) are divalent and trivalent cations respectively; A^{n-} is an anion including CI^-, Br^-, CO_3^{2-}, NO_3^-, SO_4^{2-},$[Fe(CN)_6]^{3-}$, etc. The value of x is the mole fraction of M^{3+} and is generally in the range 0.2-0.33; If x is too big, it's going to form $M(OH)_3$; If x is too small, it's going to form $M(OH)_2$. Therefore, x needs to be limited within a certain range to form pure LDHs. The greatest advantage of LDHs is that its layered structure can provide abundant REDOX sites, so it is suitably used as electrode materials for super-capacitors. Figure 1 illustrates the structure of LDHs. The basal spacing is defined as:

$d_{spacing} = d_{layer} + d_{inter}$,

Where d_{layer} represents the laminate thickness of the LDHs; the d_{inter} represents the height between two laminates of the LDHs.

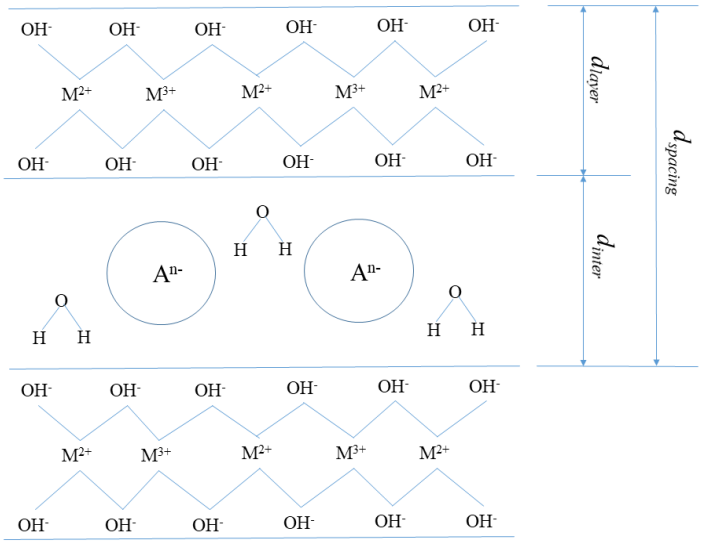

Figure 1. The structure of LDHs

In the process of electrochemical energy storage, due to the narrow basal spacing ($d_{spacing}$) of the LDHs material, the intercalation of electrolyte ions is generally inhibited, thereby limiting the full utilization of the internal structure between the layers in the electrochemical energy storage process. Xiao et al. synthesized CoAl-LDHs with different $d_{spacing}$ and tested the pseudo capacitance of super-capacitors. The results show that increasing the $d_{spacing}$ can increase the pseudo capacitance. [13].

Data mining can be adapted for material design and property optimization. [14-18] For example, Li predicted Zeta potential of decomposed peat via machine learning model. [19] Partha S. reported that the artificial neural network (ANN) model was used to predict fluoride adsorption capacity of calcined Ca-Al-(NO_3)-LDHs. [20] Hu predicted the specific surface area of LDHs by using support vector regression (SVR) model and the novel LDHs material (Ni-Fe-(CO_3)-LDHs) with the desired specific surface area was confirmed via experiments. [21] Xiong demonstrated how to predict $d_{spacing}$ of LDHs accurately via machine learning. [22] However, how to design the novel LDHs with larger $d_{spacing}$ has not been solved up to now.

In this work, the XGBoost model was constructed to screen for novel LDHs with the largest $d_{spacing}$. The result indicates that XGBoost model can be used to discover the potential LDHs with the largest $d_{spacing}$ via high throughput screening of virtual samples.

2. MATERIALS AND METHODS

2.1. Data preparation

The $d_{spacing}$ of LDHs were searched from the literatures on the web of science. [12, 23-66] The data set consisted of 85 samples with $d_{spacing}$ ranging from 6.7*Å* to 11.18*Å*. The testing set with 17 samples was randomly selected from the total data set. The rest samples were used as the training set with 68 samples.

After collecting samples, the feature candidates were collected from Lang's handbook of chemistry. [67] The table S1 lists $d_{spacing}$ data for all samples in the supporting information.

2.2. Extreme gradient boosting

The extreme gradient boosting (XGBoost) algorithm is simple in structure, small in computation and high in accuracy, which has become a very popular algorithm for machine learning in recent years. [68-72]

2.3. Metrics for model

Three metrics were adapted for evaluating machine learning model. The root mean square error (RMSE) is utilized to evaluate the deviation between the experimental and the predicted values. The mean relative error (MRE) is the mean of the relative errors. The MRE describes the deviation degree

of samples. The correlation coefficient (R) can be used to evaluate the linear correlation between the predicted and the experimental values. [73]The three metrics are defined as:

$$RMSE = \sqrt{\frac{\sum_{i=1}^{n}(p_i - e_i)^2}{n}} \quad (1)$$

$$MRE = \frac{1}{n}\sum_{i=1}^{n}\left|\frac{p_i - e_i}{e_i}\right| \quad (2)$$

$$\boldsymbol{R} = \frac{\sum(\boldsymbol{e_i}-\overline{\boldsymbol{e_i}})(\boldsymbol{p_i}-\overline{\boldsymbol{p_i}})}{\sqrt{\sum(\boldsymbol{e_i}-\overline{\boldsymbol{e_i}})^2\sum(\boldsymbol{p_i}-\overline{\boldsymbol{p_i}})^2}} \quad (3)$$

Where p_i and $e_i$are the predicted and experimental value of *i*, $\overline{p_i}$ and e_i are the predicted and experimental mean value of all samples, *n* is the number of all samples.

2.4. Computational software

The materials machine learning was implemented by using the ExpMiner (Data mining software package) and OCPMDM (online computation platform for materials data mining) developed in our laboratory. [74] The ExpMiner of the trial version can be downloaded on the website: http://materials-data-mining.com/home. The OCPMDM can be available at the web address: http://materials-data-mining.com/ocpmdm.（ID: demo; password: demo）

3. RESULTS AND DISCUSSION

3.1. Flowchart of materials data mining

Figure 2 shows the materials machine learning flowchart from data collection to model explanation. Firstly, the $d_{spacing}$ of LDHs were searched from the literatures on the web of science [12, 23-66] and the feature candidates were collected from Lang's handbook of chemistry. [67]

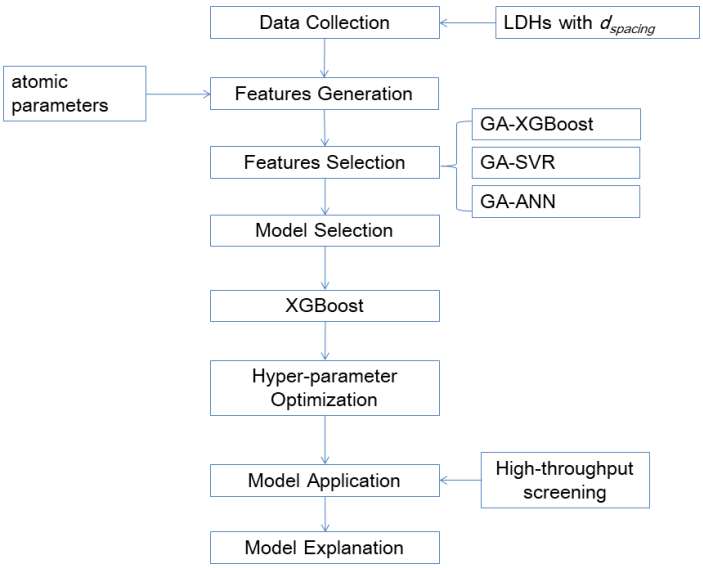

Figure 2. The materials data mining flowchart in this work

Secondly, the subset of optimal features was selected by using the genetic algorithm (GA) combined with machine learning approaches. [14]Then, the machine learning model based on the XGBoost method was constructed to predict the $d_{spacing}$ of LDHs. Lastly, the virtual LDHs with the largest $d_{spacing}$ were found via high throughput screening. Furthermore, the machine learning model can be explained via materials pattern recognition and sensitivity analysis. [14]

3.2. Feature selection

After data preparation, there are 19 candidate features in all for feature selection. Table S2 lists 19 candidate descriptors and the corresponding meanings in supporting information.

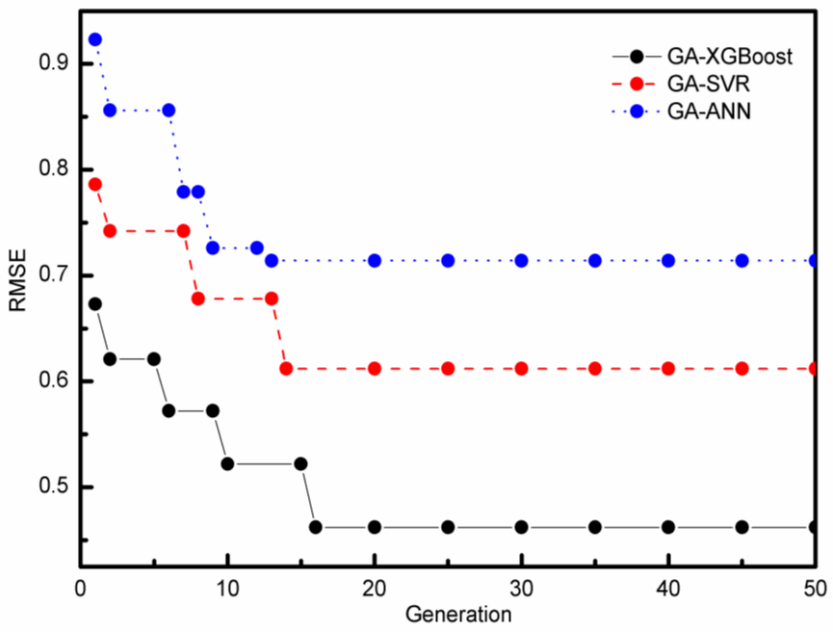

Figure 3. Feature selection by using GA-XGBoost, GA-SVR and GA-ANN, respectively

In this work, the Pearson correlation coefficient was used to calculate the correlation between feature pairs. [14] The features number selected is 15 after deletion of feature pairs with Pearson correlation coefficient larger than 0.9. Then feature selection was implemented by adopting genetic algorithm (GA) combined with three data mining approaches in model selection. [14]. The RMSE of machine learning models in LOOCV (leave one out cross-validation) was employed to evaluate the feature selection.

Figure 3 shows the results of feature selection by using GA-XGBoost, GA-SVR and GA-ANN, respectively. It can be inferred that the optimal feature subset was selected based on GA-XGBoost with the minimum RMSE. Generally, the smaller the RMSE is, the better feature subset is. Table 1 lists the corresponding meanings of 6 descriptors selected by using GA-XGBoost.

Table 1. 6 descriptors selected by using GA-XGBoost

Selected features	Meaning
TR_z	Thermochemical radii of the anion*(Å)*
N_z	The mole fraction of anions
R_a	Ionic radius of the divalent metal element*(Å)*
N_a	The mole fraction of atoms of the divalent metal element
R_b	Ionic radius of the trivalent metal element*(Å)*
E_a	Electronegativity of the divalent metal element

3.3. Model selection

The result of LOOCV was utilized to select the machine learning model. In this work, three machine learning approaches including XGBoost, SVR and ANN were adopted to establish models for predicting $d_{spacing}$ of LDHs.

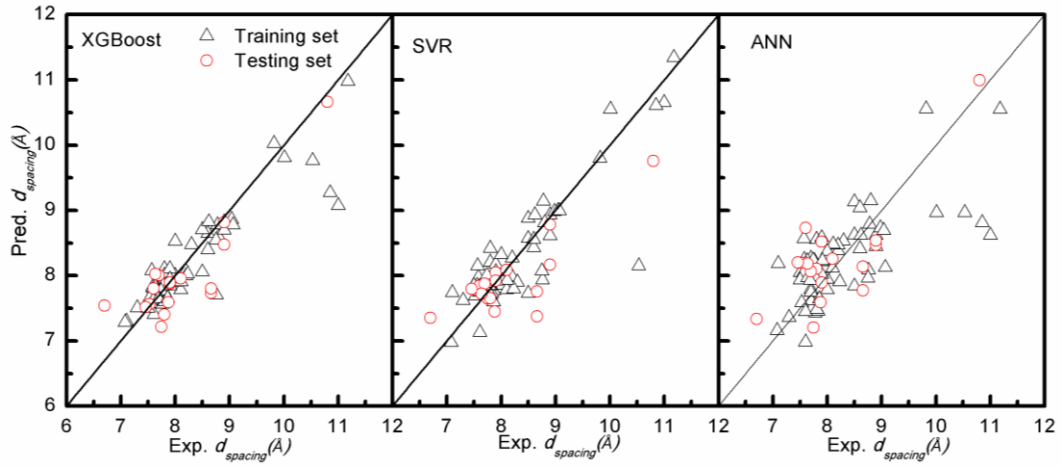

Figure 4. The Pred.$d_{spacing}$ versus Exp.$d_{spacing}$ of training set (LOOCV) and independent testing set by using XGboost, SVR, and ANN approaches, respectively

Table 2. The MRE, RMSE and R of training set (LOOCV) and independent testing set by using XGBoost, SVR, and ANN approaches, respectively

Methods	XGboost		SVR		ANN	
	training set	testing set	training set	testing set	training set	testing set
RMSE	0.39	0.44	0.42	0.52	0.47	0.53
MRE	3.72%	4.16%	3.76%	4.68	4.71%	6.26%
R	0.91	0.87	0.88	0.84	0.81	0.78

Figure 4 shows the plots of predicted $d_{spacing}$ (Pred. $d_{spacing}$) and experimental $d_{spacing}$ (Exp. $d_{spacing}$) of training set (LOOCV) and independent testing set via using XGBoost, SVR and ANN approaches, respectively. Table 2 lists the MRE, RMSE and R of training set (LOOCV) and independent testing set using XGBoost, SVR and ANN approaches, respectively. Generally, the smaller the RMSE, the better

the model is. It was concluded that the XGBoost model with the smallest RMSE outperformed SVR and ANN models.

3.4. Random sampling

To avoid contingency on account of a single sampling, three randomly sampled data sets were used to construct the XGBoost models, which were compared with the XGBoost model established above.

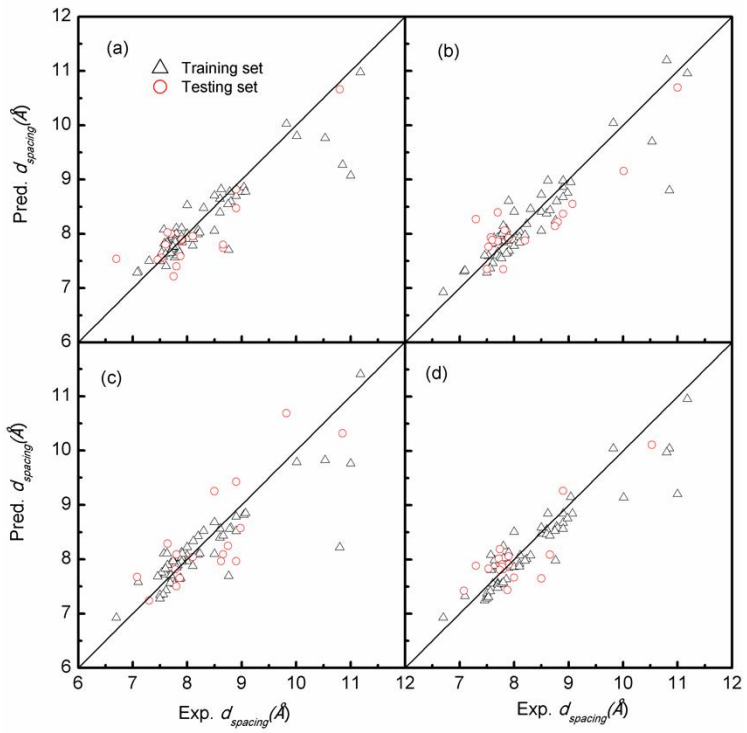

Figure 5. The Pred. $d_{spacing}$ versus Exp. $d_{spacing}$ of the training set (LOOCV) and the testing set by XGBoost, (a) the XGBoost model established above, (b-d) the XGBoost models for three random samplings

Table 3. The MRE, RMSE and R of training set (LOOCV) and testing set for the XGBoost models of four random samplings

model	samples	RMSE	MRE	R
XGBoost model established above	training set	0.39	3.72%	0.91
	testing set	0.44	4.16%	0.87
XGBoost model for the first random sampling	training set	0.38	3.81%	0.91
	testing set	0.45	4.08%	0.87
XGBoost model for the second random sampling	training set	0.37	3.67%	0.92
	testing set	0.46	4.26%	0.86
XGBoost model for the third random sampling	training set	0.41	3.87%	0.90
	testing set	0.43	4.13%	0.87
Average value of four random samples	training set	0.39	3.78%	0.91
	testing set	0.45	4.16%	0.87

Figure 5(a-d) demonstrates the plots of Pred. $d_{spacing}$ versus Exp. $d_{spacing}$ of training set (LOOCV) and testing set via using XGBoost, (a) the XGBoost model established above, (b-d) the XGBoost models for three random samplings. Table 3 lists the MRE, RMSE and R of training set (LOOCV) and testing set for the XGBoost models of four random samplings. It can be inferred that the XGBoost model is robust since there are no large differences of metrics for the training set (LOOCV) and the testing set based on different random samplings.

3.5. Hyper-parameter optimization

3.5.1. Hyper-parameter

Hyper-parameter are not arguments obtained through training, but parameters that need to be set in advance to control the learning process. In general, optimal hyper-parameters are helpful to optimize the prediction ability of machine learning model. [75]

3.5.2. Optimization methods

Table 4. The hyper-parameter optimized via Bayesian optimization.

Main hyper-parameter	Space	Step	Distribution	Optimal value
n_estimators	[40,100]	10	Quniform	70
max_depth	[3,12]	1	Quniform	4
min_samples_leaf	[2,10]	1	Quniform	3
min_samples_split	[2,20]	1	Quniform	6
learning_rate	[0.05,0.4]	0.05	Loguniform	0.25
Subsample	[0.1,0.8]	0.1	Uniform	0.6

The common methods of hyper-parameter optimization are random search, grid search, genetic algorithm optimization and Bayesian optimization. Bayesian optimization refers to previous evaluations when trying the next set of hyper-parameters. Therefore, so it can save a lot of useless work. [76]The optimal values selected by Bayesian optimization are shown in Table 4.

3.6. Validation of optimal model

After hyper-parameter optimization, the MRE, RMSE and R of the testing set and the training set were adopted to estimate the generalization performance of the optimal model.

Figure 6 illustrates the plots of the Pred.$d_{spacing}$ versus Exp.$d_{spacing}$ based on the optimal XGBoost model in the training set (LOOCV). The table S3 lists the Pred.$d_{spacing}$ and Exp.$d_{spacing}$ of training set (LOOCV) in the supporting information. The MRE、RMSE and R of the training set (LOOCV) are 3.26%、 0.35、0.94, respectively.

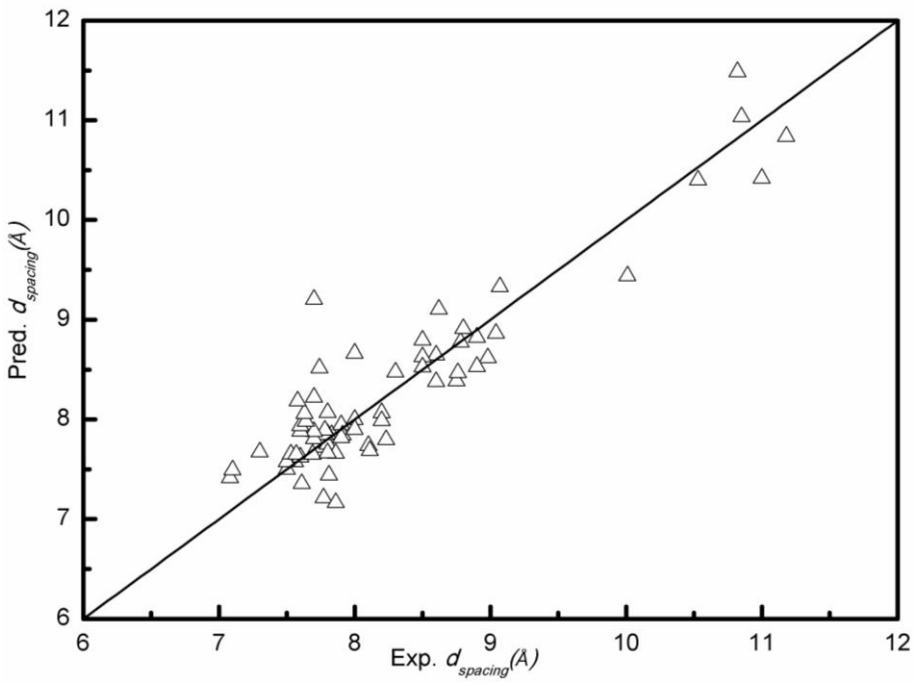

Figure 6. The Pred. $d_{spacing}$ versus Exp. $d_{spacing}$ based on the XGBoost model in LOOCV of training set

Figure 7 illustrates the plots of Pred. $d_{spacing}$ and Exp. $d_{spacing}$ of LDHs by establishing the optimal XGBoost model for independent testing set and training set, respectively. The table S4 lists the Pred. $d_{spacing}$ of the testing set in the supporting information. The MRE、RMSE and R for the modeling are 2.44%, 0.11, 0.98, respectively. The MRE、RMSE and R of the independent testing set are 4.16%, 0.35, 0.89, respectively. In general, the smaller the MRE is, the better the performance of the model is.

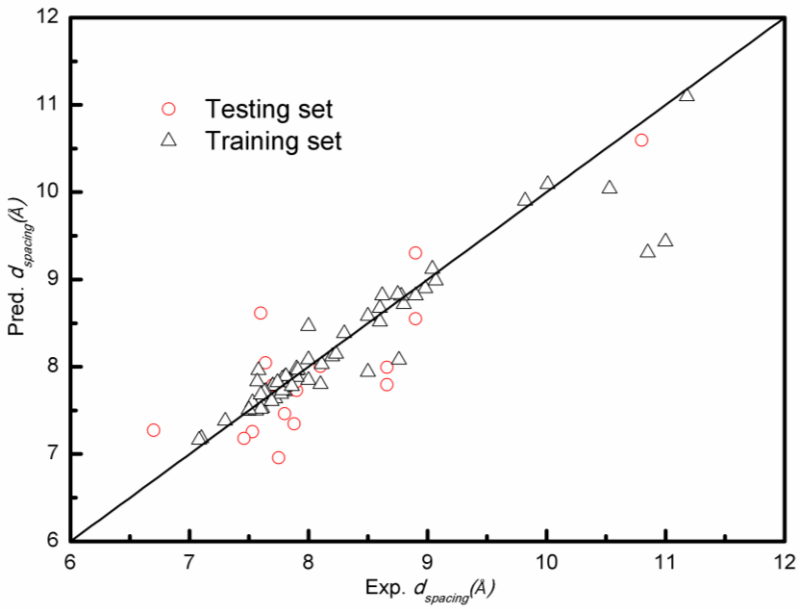

Figure 7. The Pred. $d_{spacing}$ versus Exp. $d_{spacing}$ of training dataset and independent testing dataset by using XGBoost

To further validate our model, the above established XGBoost model was used to test whether it can accurately predict our previous experiment [22, 74] and newly literature reported data in 2020 [77-83]. Table.5 list the experimental and predicted $d_{spacing}$ of our previous experiment and reported data. The MRE values between the experimental and predicted $d_{spacing}$ values is 4.13%.

Table 5. The Exp. $d_{spacing}$ and Pred. $d_{spacing}$ of our previous experimental and literature reported data

formula	Exp.$d_{spacing}$ (*Å*)	Pred. $d_{spacing}$ (*Å*)	Ref.
$Mg_{0.65}Al_{0.35}(NO_3)_{0.35}$	7.51	7.59	[22]
$Ni_{0.65}Al_{0.33}(CO3)_{0.17}$	7.68	7.45	[74]
$Ni_{0.75}Mn_{0.25}(NO_3)_{0.25}$	7.38	7.51	[77]
$Mg_{0.67}Fe_{0.33}(NO_3)_{0.33}$	7.74	7.76	[78]
$Ca_{0.67}Al_{0.33}(NO_3)_{0.33}$	8.58	8.23	[79]
$Cu_{0.75}Cr_{0.25}(NO_3)_{0.25}$	7.68	8.7	[80]
$Ni_{0.67}Fe_{0.33}(Cl)_{0.33}$	7.67	7.59	[81]
$Ni_{0.75}Mn_{0.25}(Cl)_{0.25}$REF	7.91	7.15	[82]
$Ni_{0.67}Fe_{0.33}(NO3)_{0.33}$b	7.79	8.13	[83]

3.7. Model application

3.7.1. Virtual Screening

The XGBoost model is proved to be able to accurately predict $d_{spacing}$ of LDHs. So, the XGBoost model was combined with the OCPMDM that can be used for screening out the novel LDHs with larger $d_{spacing}$ among numerous candidate materials. One the basis of the formula of LDHs, altogether 11000 candidates were generated.

Table 6 lists 5 potential candidate LDHs with larger $d_{spacing}$ screened out by using the XGBoost model available. The largest $d_{spacing}$ of designed LDHs ($Co_{0.67}Fe_{0.33}[Fe(CN)_6]_{0.11}\bullet(OH)_2$) was predicted to be 12.40*Å*, increasing by 10.91% compared to the maximum $d_{spacing}$ of $Mg_{0.67}Al_{0.33}[Fe(CN)_6]_{0.08}\bullet(OH)_2$ (11.18*Å*) reported. The mole fraction of trivalent cations in the virtual sample was recorded to verify the formation of pure LDHs.

Table 6. The potential candidate LDHs with larger Pred.$d_{spacing}$ screened out by using the XGBoost model available

Molecular formula	Pred.$d_{spacing}$	Mole fraction
$Co_{0.67}Fe_{0.33}[Fe(CN)_6]_{0.11}\bullet(OH)_2$	12.40	0.33
$Co_{0.75}Fe_{0.25}[Fe(CN)_6]_{0.08}\bullet(OH)_2$	11.80	0.25
$Ni_{0.67}Fe_{0.33}[Fe(CN)_6]_{0.11}\bullet(OH)_2$	11.72	0.33
$Ni_{0.67}Fe_{0.33}[MoO_4]_{0.17}\bullet(OH)_2$	11.66	0.33
$Co_{0.75}Al_{0.25}[Fe(CN)_6]_{0.08}\bullet(OH)_2$	11.62	0.25

3.7.2. Online Prediction

The online prediction platform based on the XGBoost model can help the experimental scientists to quickly predict the $d_{spacing}$ of new LDHs. Figure 8 shows the online platform for predicting $d_{spacing}$ of LDHs. User only need to input the formula of LDHs and click the 'predict' button to obtain the $d_{spacing}$. [14]The online prediction platform can be accessible at the web address: http://materials-data-mining.com/online_model/LDHs_basal_spacing_model.

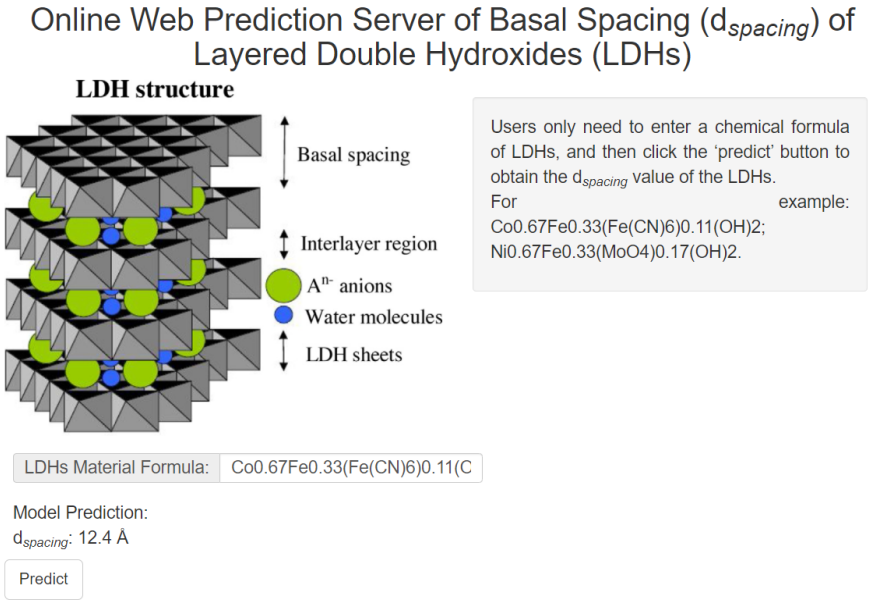

Figure 8. The online platform for predicting $d_{spacing}$ of LDHs

3.8. Model explanation

3.8.1. Materials pattern recognition

Material pattern recognition such as Fisher discriminant analysis (FDA) was used to interpret five virtual promising candidate LDHs samples. [84] Pattern recognition is based on the principle that birds of a feather flock together. Figure 9 illustrates the classification diagram of pattern recognition of different types of LDHs by employing FDA method. The samples with $d_{spacing}$ larger than 8Å were tagged as red circle (○), while the other samples are tagged as black triangle (△). It can be found that the five promising candidate LDHs tagged as green square (■) are projected in the area of circle samples in Figure 9. The distribution of the five promising candidate LDHs accords with the classification regularity based on FDA. The result of FDA verifies that the five promising candidate LDHs are located in the optimal region of pattern recognition diagram.

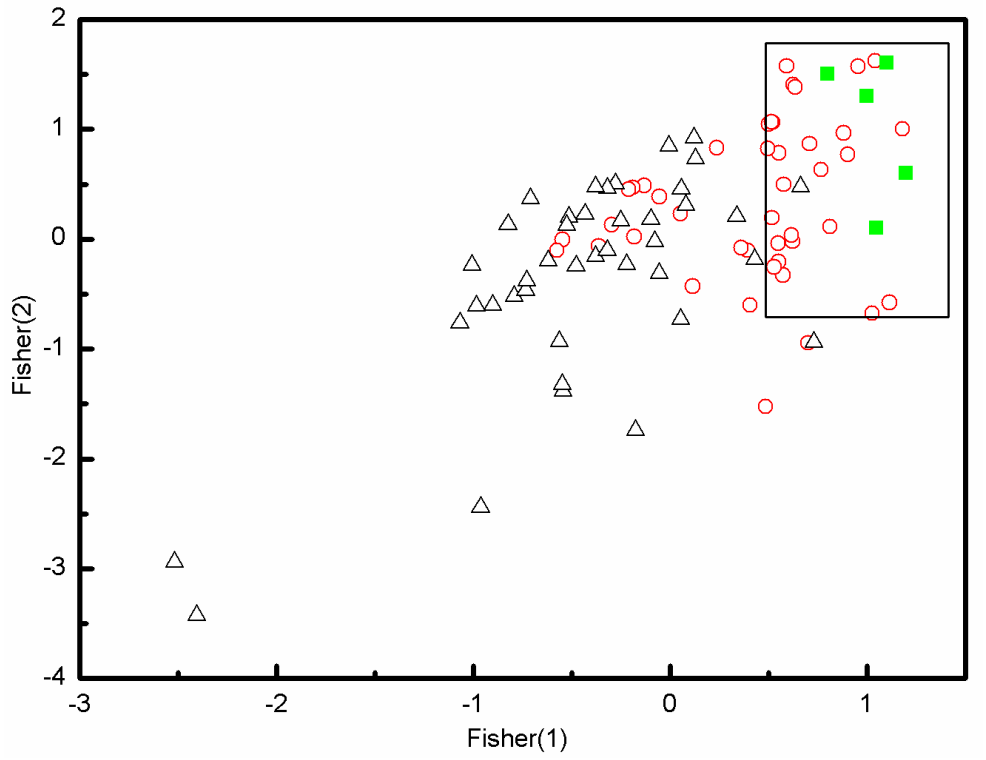

(○): The samples with the larger $d_{spacing}$

(△): The samples with the smaller $d_{spacing}$

(■): The virtual samples

Figure 9. Materials pattern recognition of different types of samples by using FDA

3.8.2. Sensitivity analysis

Sensitivity analysis is widely utilized in materials machine learning. It can be applied to observe the tendency of object variable depending single feature while the other features are constant. [14]Six key features based on GA-XGBoost method are screened to draw the figures of sensitivity analysis. Figure 10(a-f) shows sensitivity analysis of selected features, including thermochemical radii of the anion*(Å)*, the mole number of anions, ionic radius of the divalent metal element*(Å)*, the mole number of atoms of the divalent metal element, ionic radius of the trivalent metal element*(Å)* and electronegativity of the divalent metal element, respectively.

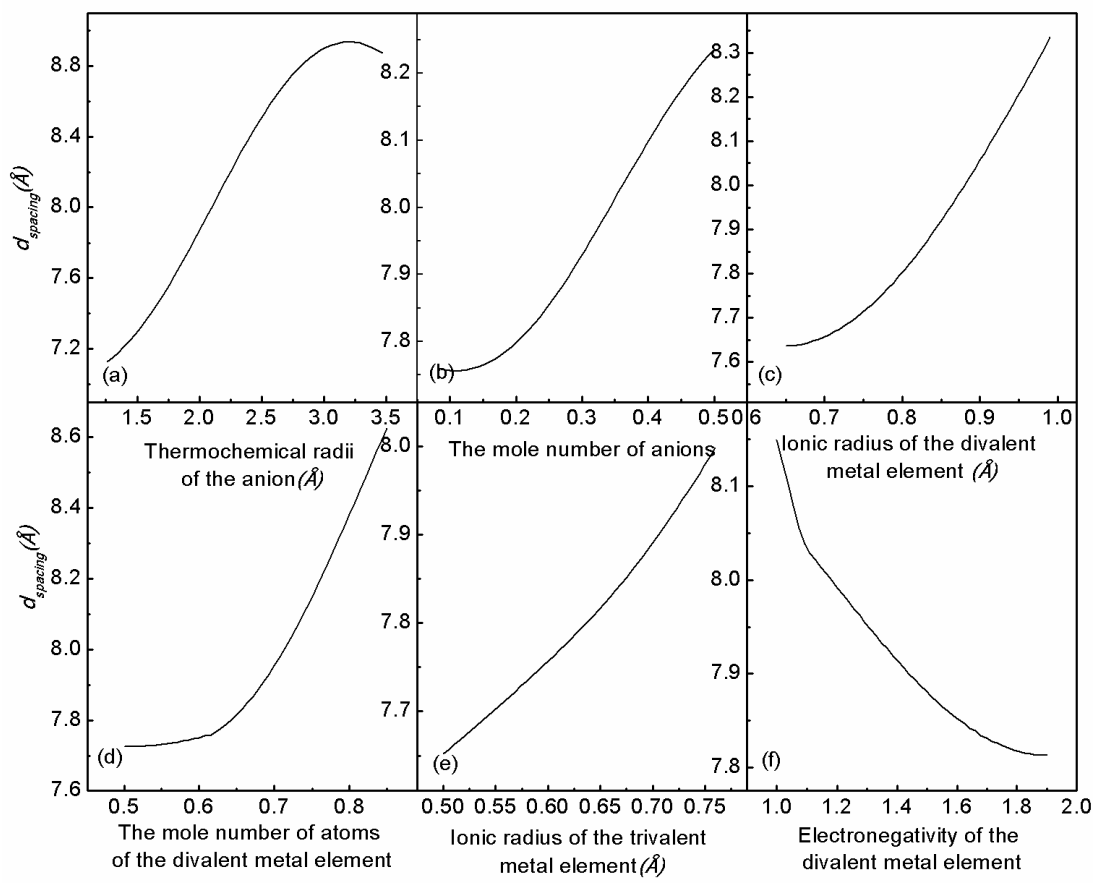

Figure 10.（a-f） Sensitivity analysis of selected features (a)Thermochemical radii of the Anion*(Å)*, (b)The mole number of anions, (c)Ionic radius of the divalent metal element*(Å)*, (d)The mole number of the divalent metal element, (e)Ionic radius of the trivalent metal element*(Å)*, and (f)Electronegativity of the divalent metal element, respectively

From the structure of LDHs (see Figure 1), it can be seen that the size and number of anions will affect the size of the d_{inter}. The larger the thermochemical radius and the mole fraction of anion is, the larger the d_{inter} is, which agrees to Figure 10(a, b). In the same way, the larger the radius and the mole fraction of metal cation is, the larger the d_{layer} is, which corresponds to figure 10(c, d, e). The more electronegative the metal cation is, the closer the metal cation is bound to anion. Therefore, electronegative of the divalent metal element are negatively correlated with d_{layer}, which is shown in figure 10(f).

3.9. Potential application of predicted materials

It was reported that the pseudo-capacitances can be increased with the expansion of $d_{spacing}$. [13]. It can be concluded that larger basal spacing allows more electrolyte ions to be stored, resulting in a higher electrochemical activity. Therefore, it is possible to apply $CoFe(Fe(CN)_6)$–LDHs (12.4 *Å* , designed LDHs with lager $d_{spacing}$) in a super-capacitors.

4. CONCLUSION

In summary, the $d_{spacing}$ of LDHs was predicted conveniently by XGBoost model on the online platform for predicting $d_{spacing}$ of LDHs. Based on the developed machine learning model and OCPMDM platform, we predicted new LDHs $(Co_{0.67}Fe_{0.33}[Fe(CN)_6]_{0.11})\bullet(OH)_2$ with the largest $d_{spacing}$ (12.40Å), increasing by 10.91% compared to the maximum $d_{spacing}$ of $Mg_{0.67}Al_{0.33}[Fe(CN)_6]_{0.08}\bullet(OH)_2$ (11.18Å) reported. More importantly, it can be expected that machine learning methods will be further applied in material design and property optimization.

ACKNOWLEDGEMENTS
Financial support to this work from the National Key Research and Development Program of China (No.2018YFB0704400) and the Science and Technology Commission of Shanghai Municipality (18520723500) is gratefully acknowledged.

SUPPORTING INFORMATION

Table S1. The dspacing data for all samples in this work
Table S2. 19 candidate features
Table S3. The experimental $d_{spacing}$ and predicted $d_{spacing}$ of training set in LOOCV
Table S4. The experimental $d_{spacing}$ and predicted $d_{spacing}$ of the testing set

Table S1. The $d_{spacing}$ data for all samples in this work

No	Molecular formula	$d_{spacing}$ (Å)
1	$Zn_{0.8}Al_{0.2}(NO_3)_{0.2}\bullet(OH)_2$	8.90
2	$Mg_{0.67}Al_{0.33}(NO_3)_{0.33}\bullet(OH)_2$	8.90
3	$Mg_{0.75}Al_{0.25}(NO_3)_{0.25}\bullet(OH)_2$	7.80
4	$Mg_{0.8}Al_{0.2}(NO_3)_{0.2}\bullet(OH)_2$	7.90
5	$Mg_{0.68}Al_{0.32}(CO_3)_{0.16}\bullet(OH)_2$	7.61
6	$Ni_{0.66}Al_{0.34}(CO_3)_{0.17}\bullet(OH)_2$	7.50
7	$Zn_{0.68}Al_{0.32}(CO_3)_{0.16}\bullet(OH)_2$	7.53
8	$Zn_{0.75}Al_{0.25}(Cl)_{0.25}\bullet(OH)_2$	7.86
9	$Cu_{0.67}Cr_{0.33}(Cl)_{0.33}\bullet(OH)_2$	7.80
10	$Zn_{0.9}1Ti_{0.09}(CO_3)_{0.045}\bullet(OH)_2$	6.70
11	$Zn_{0.8}Al_{0.2}(SO_4)_{0.1}\bullet(OH)_2$	11.00
12	$Mg_{0.67}Al_{0.33}[Fe(CN_6)]_{0.11}\bullet(OH)_2$	11.18
13	$Mg_{0.75}Al_{0.25}[Fe(CN_6)]_{0.083}\bullet(OH)_2$	9.82
14	$Ni_{0.75}Ti_{0.25}(CO_3)_{0.125}\bullet(OH)_2$	7.75
15	$Mg_{0.73}Al_{0.27}(CO_3)_{0.135}\bullet(OH)_2$	7.80
16	$Mg_{0.8}Fe_{0.2}(Cl)_{0.2}\bullet(OH)_2$	7.88
17	$Mg_{0.8}Fe_{0.2}(CO_3)_{0.1}\bullet(OH)_2$	8.00
18	$Ca_{0.67}Al_{0.33}(NO_3)_{0.33}\bullet(OH)_2$	8.80
19	$Zn_{0.65}Al_{0.35}(NO_3)_{0.35}\bullet(OH)_2$	7.90
20	$Mg_{0.66}Al_{0.34}(CO_3)_{0.17}\bullet(OH)_2$	7.58
21	$Ni_{0.67}Al_{0.33}(ClO_4)_{0.33}\bullet(OH)_2$	8.78
22	$Ni_{0.75}Al_{0.25}(ClO_4)_{0.25}\bullet(OH)_2$	8.98
23	$Ni_{0.8}Al_{0.2}(ClO_4)_{0.2}\bullet(OH)_2$	9.04

24	$Ni_{0.67}Al_{0.33}(CO_3)_{0.165}\bullet(OH)_2$	7.56
25	$Ni_{0.75}Al_{0.25}(CO_3)_{0.125}\bullet(OH)_2$	7.72
26	$Ni_{0.8}Al_{0.2}(CO_3)_{0.1}\bullet(OH)_2$	7.74
27	$Mg_{0.5}Al_{0.5}(CO_3)_{0.25}\bullet(OH)_2$	7.70
28	$Ni_{0.83}Ti_{0.17}(CNO)_{0.17}\bullet(OH)_2$	7.30
29	$Cu_{0.67}Cr_{0.33}(NO_3)_{0.33}\bullet(OH)_2$	9.07
30	$Ni_{0.67}Al_{0.33}(NO_3)_{0.33}\bullet(OH)_2$	8.60
31	$Mg_{0.67}Al_{0.33}(WO_4)_{0.165}\bullet(OH)_2$	10.01
32	$Mg_{0.68}Al_{0.32}(WO4)_{0.16}\bullet(OH)_2$	10.53
33	$Cu_{0.67}Al_{0.33}(NO_3)_{0.33}\bullet(OH)_2$	7.60
34	$Zn_{0.67}Fe_{0.33}(NO_3)_{0.33}\bullet(OH)_2$	8.10
35	$Zn_{0.67}Fe_{0.33}(MoO_4)_{0.165}\bullet(OH)_2$	8.20
36	$Ni_{0.5}Fe_{0.5}(F)_{0.50}\bullet(OH)_2$	7.60
37	$Ni_{0.5}Fe_{0.5}(Cl)_{0.50}\bullet(OH)_2$	7.80
38	$Ni_{0.5}Fe_{0.5}(Br)_{0.50}\bullet(OH)_2$	8.00
39	$Ni_{0.5}Fe_{0.5}(I)_{0.50}\bullet(OH)_2$	8.10
40	$Ni_{0.5}Fe_{0.5}(SO_3)_{0.25}\bullet(OH)_2$	8.50
41	$Ni_{0.5}Fe_{0.5}(S_2O_3)_{0.25}\bullet(OH)_2$	8.30
42	$Ni_{0.5}Fe_{0.5}(S_2O_8)_{0.25}\bullet(OH)_2$	8.50
43	$Ni_{0.5}Fe_{0.5}(CO_3)_{0.25}\bullet(OH)_2$	7.70
44	$Ni_{0.5}Fe_{0.5}(ClO)_{0.50}\bullet(OH)_2$	7.70
45	$Ni_{0.5}Fe_{0.5}(ClO_2)_{0.50}\bullet(OH)_2$	7.90
46	$Ni_{0.5}Fe_{0.5}(ClO_3)_{0.50}\bullet(OH)_2$	7.90
47	$Ni_{0.5}Fe_{0.5}(ClO_4)_{0.50}\bullet(OH)_2$	8.20
48	$Ni_{0.5}Fe_{0.5}(NO_2)_{0.50}\bullet(OH)_2$	7.90
49	$Co_{0.75}Cr_{0.25}(NO_3)_{0.25}\bullet(OH)_2$	8.66
50	$Mn_{0.75}Fe_{0.25}(NO_3)_{0.25}\bullet(OH)_2$	7.10
51	$Ni_{0.5}Al_{0.5}(NO_3)_{0.5}\bullet(OH)_2$	8.90
52	$Ni_{0.5}Al_{0.5}(Cl)_{0.25}\bullet(OH)_2$	7.70
53	$Ni_{0.5}Al_{0.5}(CO_3)_{0.25}\bullet(OH)_2$	7.70
54	$Zn_{0.75}Al_{0.25}(CO_3)_{0.125}\bullet(OH)_2$	7.64
55	$Zn_{0.75}Al_{0.25}(SO_4)_{0.125}\bullet(OH)_2$	8.50
56	$Ni_{0.75}Fe_{0.25}(CO_3)_{0.125}\bullet(OH)_2$	7.53
57	$Ni_{0.75}Fe_{0.25}(Cl)_{0.25}\bullet(OH)_2$	7.78
58	$Ni_{0.75}Fe_{0.25}(NO_3)_{0.25}\bullet(OH)_2$	8.23
59	$Ca_{0.82}Al_{0.18}(NO_3)_{0.18}\bullet(OH)_2$	8.60
60	$Co_{0.75}Fe_{0.25}(Cl)_{0.25}\bullet(OH)_2$	7.83
61	$Mg_{0.85}Al_{0.15}(NO_3)_{0.15}\bullet(OH)_2$	8.11
62	$Zn_{0.67}Al_{0.33}(NO_3)_{0.33}\bullet(OH)_2$	7.57
63	$Co_{0.67}Mn_{0.33}(NO_3)_{0.33}\bullet(OH)_2$	7.80
64	$Co_{0.67}Mn_{0.33}(Cl)_{0.33}\bullet(OH)_2$	7.60
65	$Co_{0.67}Mn_{0.33}(SO_4)_{0.165}\bullet(OH)_2$	10.80
66	$Co_{0.66}Al_{0.34}(NO_3)_{0.34}\bullet(OH)_2$	8.90
67	$Co_{0.66}Al_{0.34}(CO_3)_{0.17}\bullet(OH)_2$	7.50
68	$Mg_{0.67}Al_{0.33}(NO_3)_{0.33}\bullet(OH)_2$	8.62
69	$Ca_{0.67}Fe_{0.33}(Cl)_{0.33}\bullet(OH)_2$	7.77
70	$Mg_{0.67}Al_{0.33}(Cl)_{0.33}\bullet(OH)_2$	8.66
71	$Zn_{0.67}Al_{0.33}(Cl)_{0.33}\bullet(OH)_2$	8.76
72	$Co_{0.67}Al_{0.33}(Cl)_{0.33}\bullet(OH)_2$	8.75
73	$Mg_{0.67}Al_{0.33}(H_2PO_4)_{0.33}\bullet(OH)_2$	10.85

74	$Zn_{0.67}Al_{0.33}(CO_3)_{0.17}•(OH)_2$	7.46
75	$Zn_{0.8}Ti_{0.2}(Cl)_{0.2}•(OH)_2$	7.08
76	$Ni_{0.67}Fe_{0.33}(NO_3)_{0.33}•(OH)_2$	7.64
77	$Ni_{0.67}Fe_{0.33}(VO_3)_{0.33}•(OH)_2$	7.78
78	$Ni_{0.67}Fe_{0.33}(MoO_4)_{0.165}•(OH)_2$	7.63
79	$Ni_{0.73}Al_{0.27}(NO_3)_{0.27}•(OH)_2$	8.00
80	$Zn_{0.67}Cr_{0.33}(Cl)_{0.33}•(OH)_2$	7.81
81	$Mg_{0.75}Al_{0.25}(CO_3)_{0.125}•(OH)_2$	7.74
82	$Mg_{0.8}Al_{0.2}(CO_3)_{0.1}•(OH)_2$	7.91
83	$Co_{0.75}Al_{0.25}(CO_3)_{0.125}•(OH)_2$	7.69
84	$Zn_{0.75}Ga_{0.25}(Cl)_{0.25}•(OH)_2$	7.86
85	$Zn_{0.67}Ga_{0.33}(NO_3)_{0.33}•(OH)_2$	7.60

Table S2. 19 candidate features

descriptors	Meaning
R_a	Ionic radius of the divalent metal *(*Å*)*
E_a	Electronegativity of the divalent metal element
V_a	Valence electron of the divalent metal element
D_a	Distance valence electron of the divalent metal element
W_a	Atomic weight of the divalent metal element
N_a	The mole number of the divalent metal ion
R_b	Ionic radius of the trivalent metal *(*Å*)*
E_b	Electronegativity of the trivalent metal element
V_b	Valence electron of the trivalent metal element
D_b	Distance valence electron of the trivalent metal element
W_b	Atomic weight of the trivalent metal element
$R_{a/b}$	The weighted average Ionic radius of the divalent and trivalent metal *(*Å*)*
$E_{a/b}$	The weighted average electronegativity of the divalent and trivalent metal element
$V_{a/b}$	The weighted average valence electron of the divalent and trivalent metal element
$D_{a/b}$	The weighted average distance valence electron of the divalent and trivalent metal element
$W_{a/b}$	The weighted average atomic weight of the divalent and trivalent metal element
TR_z	Thermochemical radii of the anion*(*Å*)*
W_z	Atomic weight of the anion
N_z	The mole number of anions

Table S3. The experimental $d_{spacing}$ and predicted $d_{spacing}$ of training set in LOOCV

No.	Experimental $d_{spacing}$ (Å)	Predicted $d_{spacing}$ (Å)
2	8.9	8.82
3	7.8	7.88

5	7.61	7.53
6	7.5	7.49
8	7.86	7.78
9	7.8	7.88
11	11	9.43
12	11.18	11.1
13	9.82	9.9
17	8	8.08
18	8.8	8.72
19	7.9	7.96
20	7.58	7.96
21	8.78	8.81
22	8.98	8.9
23	9.04	9.12
24	7.56	7.5
25	7.72	7.64
26	7.74	7.82
27	7.7	7.78
28	7.3	7.38
29	9.07	8.99
30	8.6	8.67
31	10.01	10.09
32	10.53	10.04
34	8.1	7.8
35	8.2	8.12
36	7.6	7.6
37	7.8	7.72
38	8	7.85
40	8.5	7.94
41	8.3	8.38
42	8.5	8.58
43	7.7	7.78
44	7.7	7.78
45	7.9	7.88
46	7.9	7.98
47	8.2	8.12
50	7.1	7.18
52	7.7	7.78
55	8.5	8.58
56	7.53	7.59
57	7.78	7.86
58	8.23	8.15
59	8.6	8.52
60	7.83	7.85
61	8.11	8.03
62	7.57	7.83
63	7.8	7.77
64	7.6	7.52
66	8.9	8.82
67	7.5	7.51

68	8.62	8.82
69	7.77	7.69
71	8.76	8.08
72	8.75	8.83
73	10.85	9.31
75	7.08	7.16
76	7.64	7.72
77	7.78	7.73
78	7.63	7.71
79	8	8.47
80	7.81	7.89
81	7.74	7.82
82	7.91	7.96
83	7.69	7.61
84	7.86	7.78
85	7.6	7.68

Table S4. The experimental $d_{spacing}$ and predicted $d_{spacing}$ of the testing set

No	Experimental $d_{spacing}$ (Å)	Predicted $d_{spacing}$ (Å)
1	8.9	8.55
4	7.9	7.73
7	7.53	7.26
10	6.7	7.27
14	7.75	6.96
15	7.8	7.46
16	7.88	7.35
33	7.6	8.61
39	8.1	8.01
48	7.9	7.83
49	8.66	7.99
51	8.9	9.3
53	7.7	7.79
54	7.64	8.05
65	10.8	10.6
70	8.66	7.79
74	7.46	7.18

References

1 A. Seijas-Da Silva, R. Sanchis-Gual, J. A. Carrasco, V. Oestreicher, G. Abell, E. Coronado. *Batteries Supercaps*., 3 (2020) 499-509.
2 N. Ashraf, M. I. Khan, A. Majid, M. Rafique, M. B. Tahir, *Chin. J. Phys*., 66 (2020) 246-257.
3 Y. Ouyang, T. Xing, Y. Chen, L. Zheng, J. Peng, C. Wu, B. Chang, Z. Luo, X. Wang, *J. Energy Storage*., 30 (2020) 16-21.
4 T. Wang, F. Yu, X. Wang, S. Xi, K.-J. Chen, H. Wang, *Electrochim. Acta*., 334 (2020) 56-62.
5 J. Zhao, C. Ge, Z. Zhao, Q. Wu, M. Liu, M. Yan, L. Yang, X. Wang, Z. Hu, *Nano Energy*., 76 (2020) 74-78.
6 H. Chen, L. F. Hu, M. Chen, Y. Yan, L. M. Wu, *Adv. Funct. Mater.*, 24 (2014) 934-942.

7 P. Simon, Y. Gogotsi, *Nat. Mater.*, 7 (2008) 845-854.
8 P.-C. Chen, G. Shen, Y. Shi, H. Chen, C. Zhou, *ACS Nano*., 4 (2010) 4403-4411.
9 J. Huang, B. G. Sumpter, V. Meunier, *Angew. Chem. Int. Ed*., 47 (2008) 520-524.
10 M. Inagaki, H. Konno, O. Tanaike, *J. Power Sources*., 195 (2010) 7880-7903.
11 L. L. Zhang, X. S. Zhao, *Chem. Soc. Rev.*, 38 (2009) 2520-2531.
12 P. Nalawade, B. Aware, V. Kadam, R. Hirlekar.2009.
13 Y. Xiao, D. Su, X. Wang, S. Wu, L. Zhou, S. Fang, F. Li, *Sci. China Mater.*, 61 (2017) 263-272.
14 J. Roberts, Y. Song, M. Crocker, C. Risko, *J. Chem. Inf. Model.*, 60 (2020) 4845-4855.
15 W. Lu, R. Xiao, J. Yang, H. Li, W. Zhang, *J. Materiomics*., 3 (2017) 191-201.
16 Y. Liu, T. Zhao, W. Ju, S. Shi, *J. Materiomics*., 3 (2017) 159-177.
17 Q. Tao, P. Xu, M. Li, W. Lu, *npj Comput. Mater.*, 7 (2021) 117-185.
18 P. V. Balachandran, *MRS Bull.*, 45 (2020) 579-586.
19 H. Li, F. D. Chen, K. W. Cheng, Z. Z. Zhao, D. Z. Yang, *Int. J. Electrochem. Sci.*, 10 (2015) 6044-6056.
20 P. S. Ghosal, A. K. Gupta, *J. Mol. Liq.*, 222 (2016) 564-570.
21 B. Hu, K. L. Lu, Q. Zhang, X. B. Ji, W. C. Lu, *Comput. Mater. Sci.*, 136 (2017) 29-35.
22 P. Xiong, X. Ji, X. Zhao, W. Lv, T. Liu, W. Lu, *Chemometr Intell Lab*., 144 (2015) 11-16.
23 Q. Yin, D. M. Rao, G. J. Zhang, Y. J. Zhao, J. B. Han, K. Lin, L. R. Zheng, J. Zhang, J. S. Zhou, M. Wei, *Adv. Funct. Mater.*, 29 (2019) 9-12.
24 M. Szabados, Z. Kónya, Á. Kukovecz, P. Sipos, I. Pálinkó, *Appl. Clay Sci.*, 174 (2019) 138-145.
25 E. P. Rebitski, M. Darder, P. Aranda, *Beilstein J Nanotechnol*., 10 (2019) 1679-1690.
26 M. Qin, S. Li, Y. Zhao, C.-Y. Lao, Z. Zhang, L. Liu, F. Fang, H. Wu, B. Jia, Z. Liu, W. A. Wang, Y. Liu, X. Qu, *Adv. Energy Mater.*, 9 (2019) 1803-1806.
27 S. A. Pawar, S. Yu, E. Ju, H. Seo, J. Yeu, J. Kim, D. S. Patil, J. C. Shin, *Appl Sci Converg Tec*., 28 (2019) 164-168.
28 X. Liu, L. Zhang, X. Gao, C. Guan, Y. Hu, J. Wang, *ACS Appl Mater Interfaces*., 11 (2019) 23236-23243.
29 M. A. Iqbal, M. Fedel, *Int. J. Miner. Metall. Mater.*, 26 (2019) 1570-1577.
30 M. Asif, A. Aziz, H. Wang, Z. Wang, W. Wang, M. Ajmal, F. Xiao, X. Chen, H. Liu, *Mikrochim. Acta*., 186 (2019) 61-69.
31 D. Zhou, Z. Cai, Y. Bi, W. Tian, M. Luo, Q. Zhang, Q. Xie, J. Wang, Y. Li, Y. Kuang, X. Duan, M. Bajdich, S. Siahrostami, X. Sun, *Nano Research*., 11 (2018) 1358-1368.
32 T. Zhan, J. Kang, X. Li, L. Pan, G. Li, W. Hou, *Sens. Actuators, B.*, 255 (2018) 2635-2642.
33 K. Nejati, A. R. Akbari, S. Davari, K. Asadpour-Zeynali, Z. Rezvani, *New J. Chem.*, 42 (2018) 2889-2895.
34 S. Yanming, L. Dongbin, L. Shifeng, F. Lihui, C. Shuai, M. A. Haque, *Arabian J. Chem.*, 10 (2017) S2295-S2301.
35 Y. Li, L. Tang, X. Ma, X. Wang, W. Zhou, D. Bai, *J. Phys. Chem. Solids*., 107 (2017) 62-67.
36 G. Huang, K. L. Zhang, S. Chen, S. H. Li, L. L. Wang, L. P. Wang, R. Liu, J. Gao, H. H. Yang, *J. Mater. Chem.*, 5 (2017) 3629-3633.
37 M. Chakraborty, M. K. Mitra, J. Chakraborty, *Bull. Mater. Sci.*, 40 (2017) 1203-1211.
38 H. Asiabi, Y. Yamini, M. Shamsayei, *J. Hazard. Mater.*., 339 (2017) 239-247.
39 S. Nagendran, G. Periyasamy, P. V. Kamath, *Dalton Trans*., 45 (2016) 18324-18332.
40 S. K. Kiran, M. Padmini, H. T. Das, P. Elumalai, *J. Solid State Electrochem.*, 21 (2016) 927-938.
41 E. Alibakhshi, E. Ghasemi, M. Mahdavian, B. Ramezanzadeh, *Progress in Color, Colorants and Coatings*., 9 (2016) 233-248.
42 Y. Jiang, X. Gu, S. Zhang, W. Tang, J. Zhao, *Mater. Lett.*, 150 (2015) 31-34.
43 J. Hu, G. Lei, Z. Lu, K. Liu, S. Sang, H. Liu, *Chem Commun (Camb)*., 51 (2015) 9983-9986.
44 S. Chakraborty, I. Sarkar, K. Haldar, S. K. Pal, S. Chakraborty, *Appl. Clay Sci.*, 107 (2015) 98-108.

45 M. N. Pahalagedara, M. Samaraweera, S. Dharmarathna, C.-H. Kuo, L. R. Pahalagedara, J. A. Gascón, S. L. Suib, *J. Phys. Chem. C.*, 118 (2014) 17801-17809.
46 Q. Wang, D. O'Hare, *Chem. Rev.*, 112 (2012) 4124-4155.
47 R. Ma, J. Liang, X. Liu, T. Sasaki, *J. Am. Chem. Soc.*, 134 (2012) 19915-19921.
48 N. Iyi, Y. Ebina, T. Sasaki, *J. Phys. Chem.*, 21 (2011) 80-85.
49 Z. Gao, B. Du, G. Zhang, Y. Gao, Z. Li, H. Zhang, X. Duan, *IND ENG CHEM RES*., 50 (2011) 5334-5345.
50 S. Fleutot, J. C. Dupin, G. Renaudin, H. Martinez, *PCCP*., 13 (2011) 17564-17578.
51 D. Chaara, F. Bruna, M. A. Ulibarri, K. Draoui, C. Barriga, I. Pavlovic, *J. Hazard. Mater*., 196 (2011) 350-9.
52 Z. P. Xu, P. S. Braterman, *Appl. Clay Sci.*, 48 (2010) 235-242.
53 S.-J. Ryu, H. Jung, J.-M. Oh, J.-K. Lee, J.-H. Choy, *J. Phys. Chem. Solids*., 71 (2010) 685-688.
54 T. Bujdosó, Á. Patzkó, Z. Galbács, I. Dékány, *Appl. Clay Sci.*, 44 (2009) 75-82.
55 J. Liu, G. Chen, J. Yang, *Polymer*., 49 (2008) 3923-3927.
56 M. S. Gasser, H. T. Mohsen, H. F. Aly, *Colloids Surf., A.*, 331 (2008) 195-201.
57 G. G. Arizaga, A. S. Mangrich, J. E. da Costa Gardolinski, F. Wypych, *J. Colloid Interface Sci.*, 320 (2008) 168-176.
58 Y. Tian, G. Wang, F. Li, D. G. Evans, *Mater. Lett.*, 61 (2007) 1662-1666.
59 P. Kovar, M. Pospisil, M. Nocchetti, P. Capkova, K. Melanova, *J. Mol. Model*., 13 (2007) 937-42.
60 N. Iyi, K. Fujii, K. Okamoto, T. Sasaki, *Appl. Clay Sci.*, 35 (2007) 218-227.
61 M. R. Pérez, I. Pavlovic, C. Barriga, J. Cornejo, M. C. Hermosín, M. A. Ulibarri, *Appl. Clay Sci.*, 32 (2006) 245-251.
62 L. Raki, J. J. Beaudoin, L. Mitchell, *Cem. Concr. Res*., 34 (2004), 1717-1724.
63 O. Saber, H. Tagaya, *J. Incl. Phenom. Macrocycl. Chem.*, 45 (2003) 109-116.
64 J. W. Boclair, P. S. Braterman, B. D. Brister, Z. Wang, F. Yarberry, *J. Solid State Chem*., 161 (2001) 249-258.
65 M. Z. bin Hussein, T. K. Hwa, *J. Nanopart. Res*., 2 (2000) 293-298.
66 M. Adachi-Pagano, C. Forano, J. P. Besse, *Chem. Commun.*, 8 (2000) 91-92.
67 J. A. Dean, *Lang's handbook of chemistry*. Editor, McGraw-Hill Book Co, 2004.
68 T. Q. Chen, C. Guestrin, M. Assoc Comp, *XGBoost: A Scalable Tree Boosting System*. Editor, Assoc Computing Machinery, New York,8 (2016) 785-794.
69 H. T. Zheng, J. B. Yuan, L. Chen, *Energies*., 10 (2017) 20-26.
70 N. Hoang, B. Xuan-Nam, B. Hoang-Bac, C. Dao Trong, *Acta Geophys*., 67 (2019) 477-490.
71 L. Torlay, M. Perrone-Bertolotti, E. Thomas, M. Baciu, *Brain informatics*., 4 (2017) 159-169.
72 D. Zhang, L. Qian, B. Mao, C. Huang, B. Huang, Y. Si, *Ieee Access*., 6 (2018) 21020-21031.
73 D.-K. Choi, *Int. J. Precis. Eng. Manuf*., 20 (2019) 129-138.
74 Q. Zhang, X. Zhai, P. Xiong, L. Kou, X. Ji, W. Lu, *Mater. Res. Bull*., 93 (2017) 123-129.
75 H. Dong, D. He, F. Wang, *Powder Technol*., 375 (2020) 174-181.
76 A. Seko, A. Togo, H. Hayashi, K. Tsuda, L. Chaput, I. Tanaka, *Phys. Rev. Lett*., 115 (2015) 119-125.
77 X. Wang, Z. Li, J. Zhang, H. Yan, C. Wang, F. Wu, A. Tian, X. Hong, W. Dong, S. Yang, *Chem. Eng. J.*, 398 (2020) 1963-1971.
78 E. Duquesne, S. Betelu, A. Seron, I. Ignatiadis, H. Perrot, C. Debiemme-Chouvy, *J. Nanomater*., 10 (2020) 1832-1836.
79 S. Saha, A. Bhattacharjee, S. H. Rahaman, A. Basu, J. Chakraborty, *Appl. Clay Sci.*, 188 (2020) 19-23.
80 M. Aghaziarati, Y. Yamini, M. Shamsayei, *Microchim. Acta*., 187 (2020) 118-124.
81 Q. Yin, J. Luo, J. Zhang, L. Zheng, G. Cui, J. Han, D. O'Hare, *J. Mater. Chem. A*., 8 (2020) 12548-12555.
82 J. Luo, Q. Yin, J. Zhang, S. Zhang, L. Zheng, J. Han, *ACS Appl. Energy Mater*., 3 (2020) 4559-

4568.
83 J. Long, J. Zhang, X. Xu, F. Wang, *Mater. Chem. Phys.*, 254 (2020) 167-174.
84 K. R. Muller, S. Mika, G. Ratsch, K. Tsuda, B. Scholkopf, *IEEE Trans. Neural Netw.*, 12 (2001) 181-201.